

## THE SDSS DAMPED Ly $\alpha$ SURVEY: DATA RELEASE 1

JASON X. PROCHASKA & STEPHANE HERBERT-FORT

UCO/Lick Observatory; University of California, 1156 High Street, Santa Cruz, CA 95064

*Submitted to the Astrophysical Journal: March 17, 2004*

### ABSTRACT

We present the results from an automated search for damped Ly $\alpha$  (DLA) systems in the quasar spectra of Data Release 1 from the Sloan Digital Sky Survey (SDSS-DR1). At  $z \approx 2.5$ , this homogeneous dataset exceeds the statistical significance of the previous two decades of research. We derive a statistical sample of 71 damped Ly $\alpha$  systems ( $> 50$  previously unpublished) at  $z > 2.1$  and measure HI column densities directly from the SDSS spectra. The number of DLA systems per unit redshift is consistent with previous measurements suggesting our survey has  $> 95\%$  completeness. We examine the cosmological baryonic mass density of neutral gas  $\Omega_g$  inferred from the damped Ly $\alpha$  systems from the SDSS-DR1 survey and a combined sample drawing from past efforts. Contrary to previous results, the  $\Omega_g$  values do not require a significant correction from Lyman limit systems at any redshift. Furthermore, the  $\Omega_g$  values for the SDSS-DR1 sample do not decline at high redshift and the combined sample shows a (statistically insignificant) decrease only at  $z > 4$ . Future data releases from SDSS will provide the definitive survey of DLA systems at  $z \approx 2.5$  and will significantly reduce the uncertainty of  $\Omega_g$  at higher redshift.

*Subject headings:* Galaxies: Evolution, Galaxies: Intergalactic Medium, Galaxies: Quasars: Absorption Lines

### 1. INTRODUCTION

It has now been two decades since the inception of surveys for high redshift galaxies through the signature of damped Ly $\alpha$  (DLA) absorption in the spectra of background quasars (Wolfe et al. 1986). Owing to large neutral hydrogen column densities  $N(\text{HI})$ , these absorption lines exhibit large rest equivalent widths  $W_\lambda > 5\text{\AA}$  and show the Lorentzian wings characteristic of quantum mechanical line-damping. Through dedicated surveys of high and low redshift quasars with optical and ultraviolet telescopes, over 300 damped Ly $\alpha$  systems have been identified. These galaxies span redshifts  $z = 0$  (the Milky Way, LMC, SMC) to  $z = 5.5$  where the opacity of the Ly $\alpha$  forest precludes detection (Songaila & Cowie 2002).

Statistics of the DLA systems impact a wide range of topics in modern cosmology, galaxy formation, and physics. These include studies on the chemical enrichment of the universe in neutral gas (Pettini et al. 1994; Prochaska et al. 2003b), nucleosynthetic processes (Lu et al. 1996; Prochaska, Howk, & Wolfe 2003), galactic velocity fields (Prochaska & Wolfe 1997), the molecular and dust content of young galaxies (Vladilo 1998; Ledoux, Srianand, & Petitjean 2003), star formation rates (Wolfe, Prochaska, & Gawiser 2003), and even constraints on temporal evolution of the fine-structure constant (Webb et al. 2001). Perhaps the most fundamental measurement from DLA surveys, however, is the evolution of the cosmological baryonic mass density in neutral gas  $\Omega_g$  (Storrie-Lombardi and Wolfe 2000; Rao & Turnshek 2000; Péroux et al. 2003, hereafter PMSI03). Because the DLA systems dominate the mass density of neutral gas from  $z = 0$  to at least  $z = 3.5$ , a census of these absorption systems directly determines  $\Omega_g$ . These measurements express global evolution in the gas which feeds star formation (Pei & Fall 1995; Mathlin et al. 2001) and are an important constraint for models of hierarchical galaxy formation (e.g. Somerville, Primack, & Faber 2001; Nagamine, Springel, & Hernquist 2004b).

The most recent compilation of damped Ly $\alpha$  systems

surveyed in a ‘blind’, statistical manner combines the effects of observing programs using over 10 telescopes, 10 unique instruments, and the data reduction and analysis of  $\approx 10$  different observers (PMSI03). In short, the results are derived from a heterogeneous sample of quasar spectra derived from heterogeneous quasar surveys. While considerable care has been paid to collate these studies into an unbiased analysis, it is difficult to assess the completeness and potential selection biases of the current sample. These issues are particularly important when one aims to address the impact of effects like dust obscuration (Ostriker & Heisler 1984; Fall & Pei 1993; Ellison et al. 2001).

In this paper we present the first results in a large survey for damped Ly $\alpha$  systems drawn from a homogeneous dataset of high  $z$  quasars with well-defined selection criteria. Specifically, we survey the quasar spectra from Data Release 1 of the Sloan Digital Sky Survey (SDSS-DR1) restricting our search to SDSS-DR1 quasars with Petrosian magnitude  $r' < 19.5$  mag. The DR1 sample alone (the first of five data releases from SDSS) offers a survey comparable to – although not strictly independent from – the efforts of 20 years of work. We introduce algorithms to automatically identify DLA candidates in the fluxed (i.e. non-normalized) quasar spectra and perform Voigt profile analyses to confirm and analyze the DLA sample. This survey was motivated by a search for ‘metal-strong’ DLA systems like the  $z=2.626$  damped Ly $\alpha$  system toward FJ0812 + 32 (Prochaska, Howk, & Wolfe 2003). A discussion of the ‘metal-strong’ survey will be presented in a future paper (Herbert-Fort et al. 2004, in preparation).

This paper is organized as follows. In § 2, we present the quasar sample and discuss the automatic DLA candidate detection. In § 3, we present the Voigt profile fits to the full sample. We present a statistical analysis in § 4 and a summary and concluding remarks are given in § 5.

### 2. QUASAR SAMPLE AND DLA CANDIDATES

The quasar sample was drawn from Data Release 1 of the Sloan Digital Sky Survey to a limiting Petrosian mag-

nitude of  $r' = 19.5$  mag. This criterion was chosen primarily to facilitate follow-up observations with 10m-class telescopes, although it does include  $> 90\%$  of all SDSS-DR1 quasars at  $z > 2$ . With rare exception, the fiber-fed SDSS spectrograph provides  $\text{FWHM} \approx 150 \text{ km s}^{-1}$  spectra of each quasar for the wavelength range  $\lambda \approx 3800 - 9200\text{\AA}$ . All of the spectra were reduced using the SDSS spectrophotometric pipeline (Burles & Schlegel 2004) and were retrieved from the SDSS data archive<sup>1</sup> (Abazajian et al. 2003).

The first step of a damped Ly $\alpha$  survey is to establish the redshift pathlength available to the discovery of DLA systems. The minimum starting wavelength of  $3800\text{\AA}$  corresponds to  $z = 2.12$  for the Ly $\alpha$  transition and this sets the lowest redshift accessible to this survey. For each quasar, however, we define a unique starting redshift  $z_{\text{start}}$  by identifying the first pixel where the median SNR over 20 pixels exceeds 4. This criterion was chosen to (1) minimize the likelihood of identifying noise features as DLA systems; (2) achieve a high completeness limit; (3) account for the presence of Lyman limit absorption. Consistent with previous studies, the ending redshift  $z_{\text{end}}$  corresponds to  $3000 \text{ km s}^{-1}$  blueward of Ly $\alpha$  emission. This criterion limits the probability of identifying DLA systems associated with the quasar which may bias the analysis.

Special consideration is given to quasar spectra which show significant absorption lines at the quasar emission redshift (e.g. CIV, O VI). In previous studies, Broad Absorption Line (BAL) quasars have been removed from the analysis primarily to prevent confusion with intrinsic O VI and/or N V absorption. We take a less conservative approach here. We visually inspected the 1252 quasars with  $z_{\text{em}} > 2.1$  and  $r' < 19.5$  to identify quasars associated absorption. In these cases, we limit the DLA search to  $100\text{\AA}$  redward of O VI emission and  $100\text{\AA}$  blueward of Ly $\alpha$  emission. However, if BAL contamination is determined to be too severe the quasar is rejected from further analysis.

The majority of previous DLA surveys relied on low resolution ‘discovery’ spectra to first identify DLA candidates. Follow-up observations were then made of these candidates to confirm DLA systems and measure their  $N(\text{HI})$  values. A tremendous advantage of the SDSS spectra is that they have sufficient resolution to both readily identify DLA candidates and measure their  $N(\text{HI})$  values. DLA candidates were identified using an algorithm tuned to the characteristics of the damped Ly $\alpha$  profile, in particular its wide, saturated core. Our DLA-searching algorithm first determines a characteristic signal-to-noise ratio (SNR) for each quasar spectrum. If Ly $\alpha$  emission (corresponding to  $z_{\text{em}}$ ) lies within the first 200 pixels of the wavelength array, the SNR is calculated to be the median flux/sigma over 150 pixels, starting 200 pixels redward of Ly $\alpha$ . Otherwise, the SNR is calculated starting 200 pixels blueward of Ly $\alpha$ . We then defined a quantity  $n_1 = \text{SNR}/2.5$  restricted to the interval [1,2]. At each pixel in the spectrum, we then measured the fraction of pixels with  $\text{SNR} < n_1$  in a window  $6(1 + z_{\text{abs}})$  pixels wide. Importantly (for fiber data), the algorithm is relatively insensitive to the effects of poor sky-subtraction. Furthermore, we stress that continuum fitting is unnecessary; the algorithm works directly on the fluxed data because it focuses

primarily on the core of the damped Ly $\alpha$  profile.

This algorithm was developed through tests on both simulated spectra with resolution and SNR comparable to SDSS data and also on a sub-set of SDSS spectra with known DLA systems. Our tests indicate that DLA candidates correspond to windows where the fraction of pixels with  $\text{SNR} < n_1$  exceeds 60%. We recorded all regions satisfying this criterion and reduced them to individual candidates by grouping within  $2000 \text{ km s}^{-1}$  bins. In a sample of 1000 trials on simulated spectra with random  $N(\text{HI})$  and redshift, we recover 100% of all DLA systems with  $\log N(\text{HI}) > 20.4$  and all but  $\approx 5\%$  of the DLA systems with  $N(\text{HI}) \approx 2 \times 10^{20} \text{ cm}^{-2}$ . The algorithm is conservative in that it triggers many false positive detections. With custom software, it is easy to visually identify and account for these cases.

Table 1 lists the full sample of SDSS-DR1 quasars. The columns give the name,  $z_{\text{em}}$ ,  $z_{\text{start}}$ ,  $z_{\text{end}}$ , a flag for BAL characteristics, and redshifts of DLA candidates including the false positive detections.

### 3. $N(\text{HI})$ ANALYSIS

The automated algorithm described in the previous section triggered 286 DLA candidates. We visually inspected the full set of candidates and identified  $\approx 100$  as obvious false positive detections. For the remainder of the systems, we fit a local continuum and a Voigt profile with  $\text{FWHM} = 2 \text{ pixels}$  to the data. The Voigt profile fits to the DLAs quoted in this paper are centered on the redshift determined by associated metal-line absorption. Because the metal lines are narrow, these redshifts are determined precisely. As emphasized by Prochaska et al. (2003a), the  $N(\text{HI})$  analysis is dominated by systematic error associated with continuum fitting and line blending of coincident Ly $\alpha$  clouds. The statistical error based on a  $\chi^2$  minimization routine would be unrealistically low and largely unmeaningful. Therefore, we perform a visual fit to the data and report a conservative systematic error which we believe encompasses an interval in  $N(\text{HI})$  corresponding to a 95% c.l. For a majority of the profiles, this corresponds to  $\pm 0.15 \text{ dex}$ , independent of  $N(\text{HI})$  value.

The Ly $\alpha$  fits for all Ly $\alpha$  profiles satisfying  $N(\text{HI}) \geq$

TABLE 1  
SDSS QUASAR SAMPLE

Name	$z_{\text{em}}$	$z_{\text{start}}$	$z_{\text{end}}$	$f_{\text{BAL}}^{\text{a}}$	$z_{\text{candidate}}$
J094454.24–004330.3	2.292	2.150	2.259	0	
J095253.84+011422.1	3.024	2.154	2.984	0	2.204, 2.381
J100412.88+001257.5	2.239	2.156	2.207	0	
J100553.34+001927.1	2.501	2.155	2.466	0	
J101014.25–001015.2	2.190	2.143	2.158	0	
J101748.90–003124.5	2.283	2.156	2.250	0	
J101859.96–005420.2	2.183	2.147	2.151	0	
J102606.67+011459.0	2.266	2.157	2.233	0	
J102636.96+001530.2	2.178	...	...	0	
J102650.39+010518.3	2.274	2.177	2.192	1	

<sup>a</sup>0=No BAL activity; 1=Modest BAL activity, included in analysis; 2=Strong BAL activity.

Note. — [The complete version of this table is in the electronic edition of the journal.]

<sup>1</sup><http://www.sdss.org>

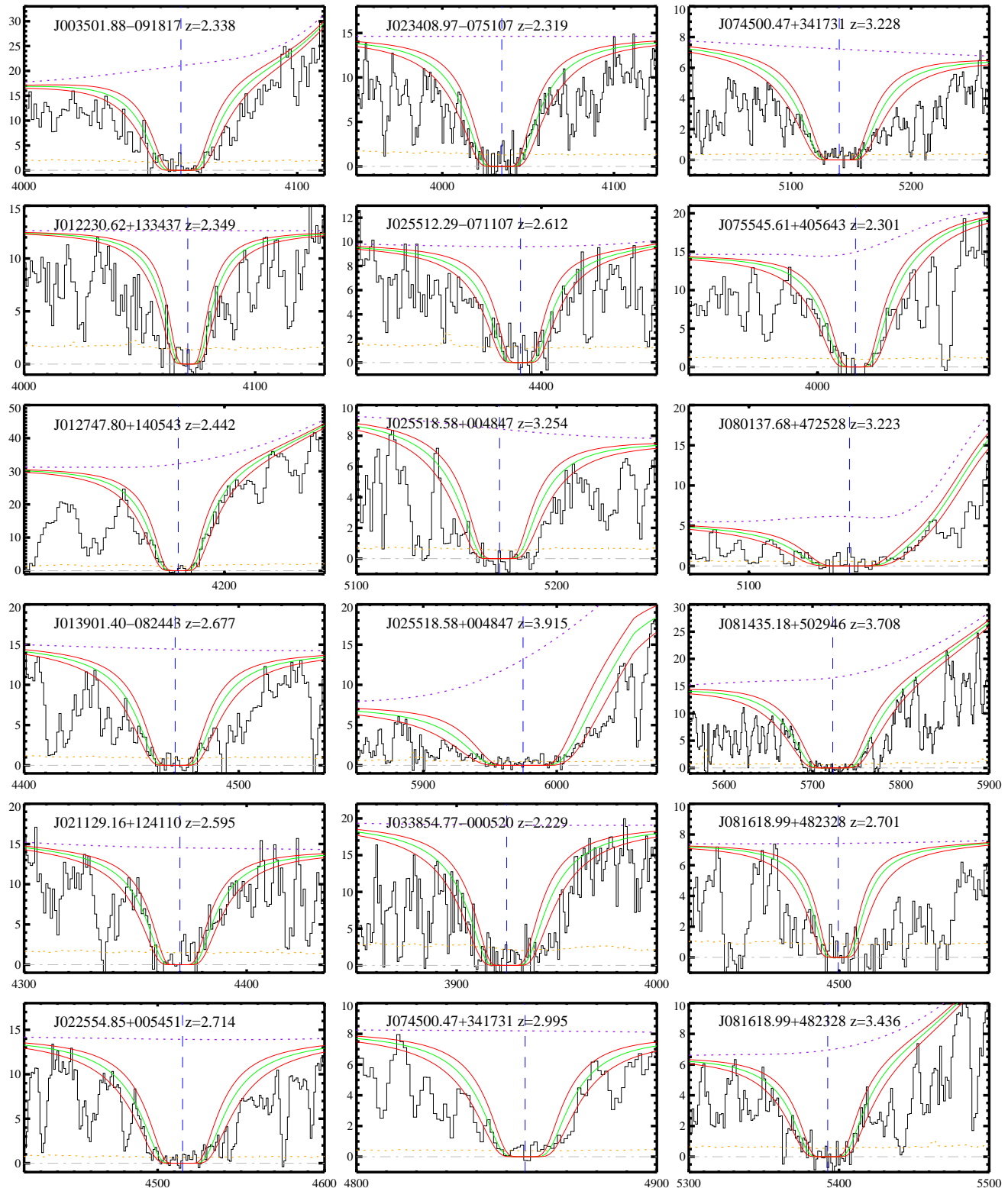
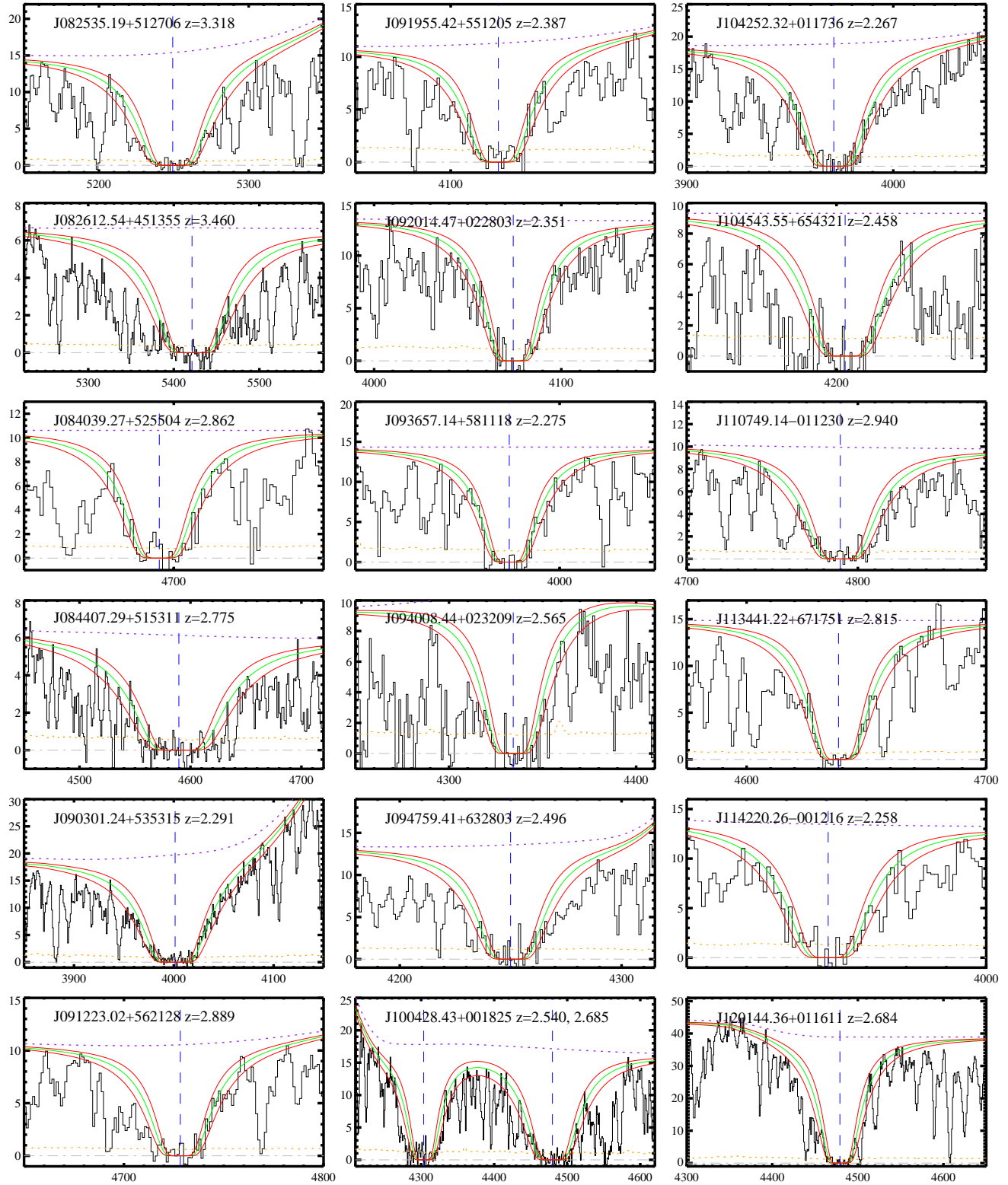
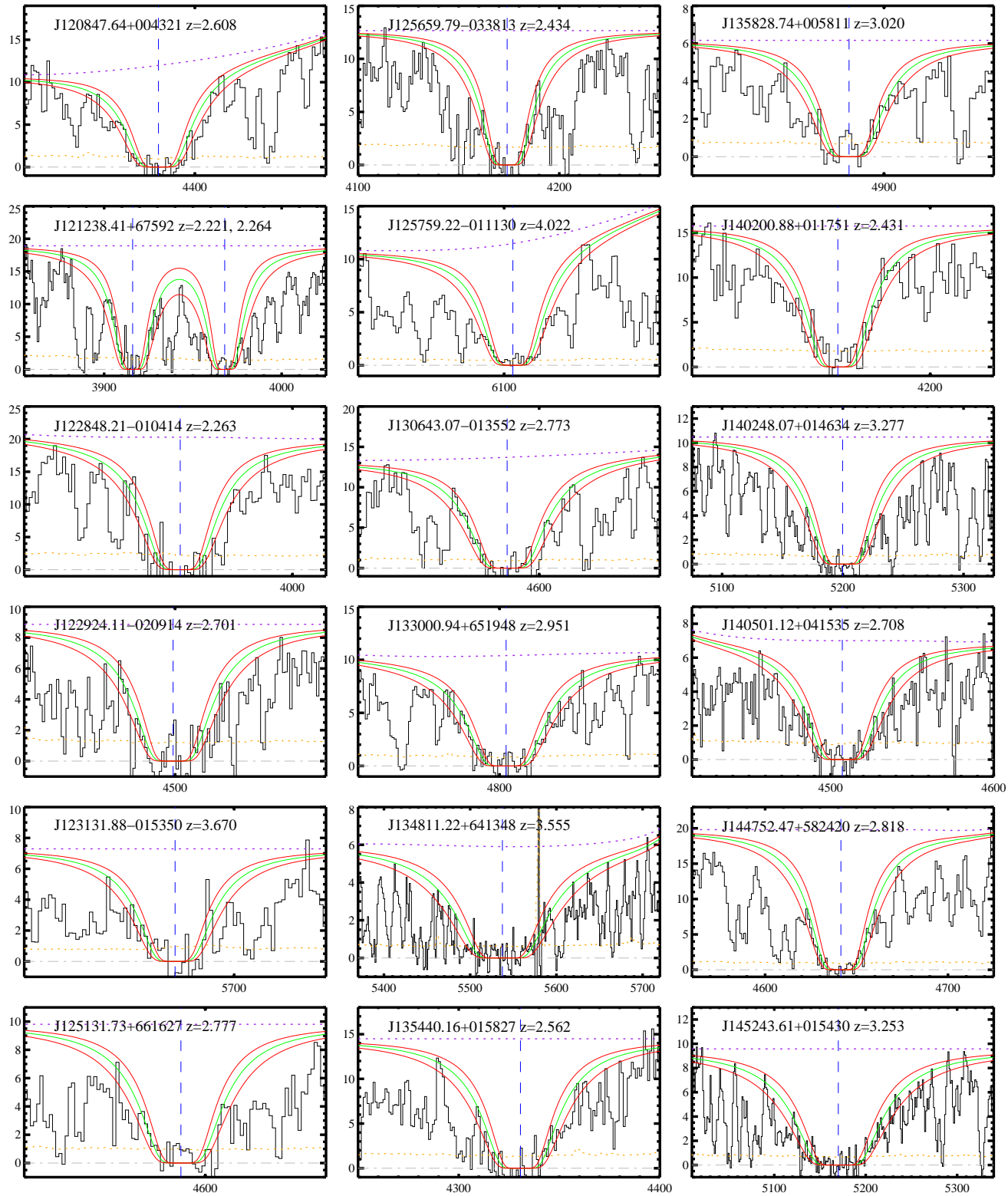
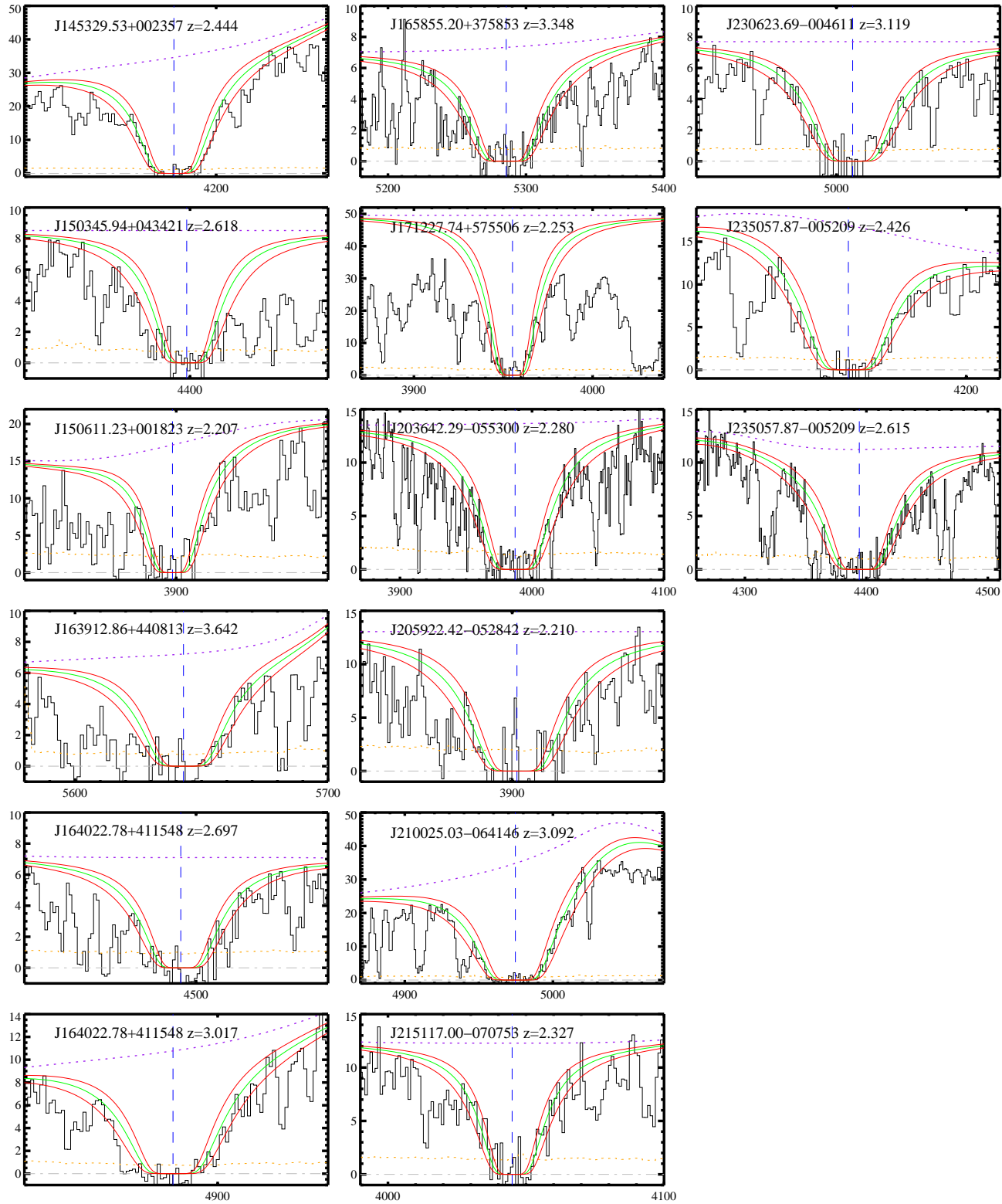


FIG. 1.— Ly $\alpha$  profiles of the 71 damped Ly $\alpha$  systems comprising the full statistical sample from the SDSS Data Release 1. The dotted line traces the assumed continuum of the quasar and the green solid line is a Voigt profile corresponding to the  $N(\text{HI})$  values given in Table 2. All plots have angstroms along the x-axis and flux ( $f_\lambda \times 10^{17}$  cgs) along the y-axis.







$2 \times 10^{20} \text{ cm}^{-2}$  criterion are plotted in Figure 2. Overplotted in each figure are the best fit and our assessment of the error corresponding to a 95% c.l. interval. Table 2 summarizes the absorption redshift,  $N(\text{HI})$  value, and systematic error and gives a brief comment for each profile (e.g. difficult continuum, severe line-blending, poor SNR).

For  $\approx 10$  of the DLA systems in the SDSSrDR1 sample, we have acquired higher resolution spectroscopy ( $FWHM \approx 30 \text{ km s}^{-1}$ ) of the Ly $\alpha$  profile with the Echellette Spectrometer and Imager (Sheinis et al. 2002) on the Keck II telescope. The ESI spectra suffer less from line blending and also allow for a more accurate determination of the quasar continuum. Furthermore, several of these systems were observed in previous studies. We find that our  $N(\text{HI})$  values agree with all previous measurements to within 0.15 dex with no systematic offset. Therefore, we are confident in the  $N(\text{HI})$  values reported here.

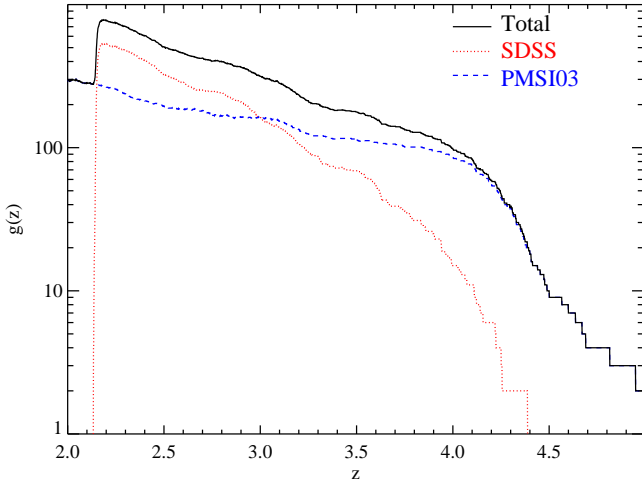


FIG. 2.— Redshift path density  $g(z)$  as a function of redshift for the (i) SDSS-DR1 survey (dotted red line); (ii) the PMSI03 compilation (dashed blue line); and (iii) the combined surveys.

#### 4. ANALYSIS

##### 4.1. $g(z)$ and $n(z)$

A simple yet meaningful description of the statistical significance of any quasar absorption line survey is given by the redshift path density  $g(z)$  (e.g. Lanzetta et al. 1991). This quantity corresponds to the number of quasars searched at a given redshift for the presence of a particular absorption feature, e.g., a damped Ly $\alpha$  system. We have constructed  $g(z)$  for the SDSS-DR1 sample by implementing the starting and ending redshifts listed in Table 1. Figure 3 presents  $g(z)$  for (i) the SDSS-DR1 sample (red dotted lines); (ii) the PMSI03 compilation (dashed blue lines); and (iii) the combined surveys taking into account overlap between the two samples (black solid line). It is evident from Figure 3 that the SDSS-DR1 sample has greatest statistical impact at  $z = 2 - 3.2$ . With only  $\approx 7\%$  of the projected SDSS database, the SDSS-DR1 exceeds the redshift path density of the previous two decades of research at  $z = 2.5$ . Although the SDSS-DR1 systems have only a modest contribution at  $z > 3$ , the projected

10 $\times$  increase in  $g(z)$  for the full SDSS sample promises a major impact for DLA studies to at least  $z = 4$ .

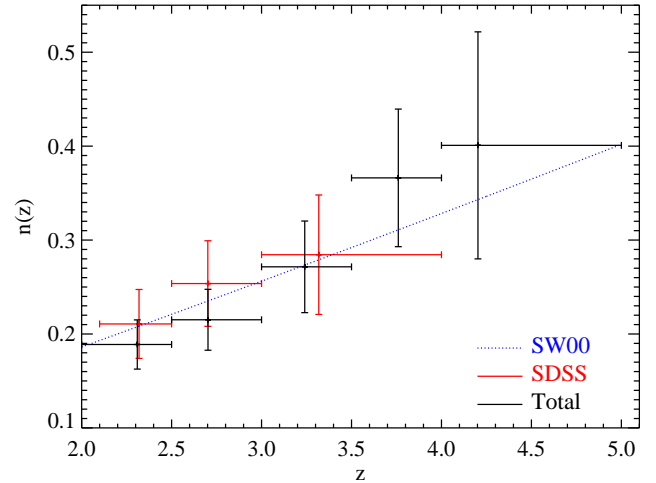


FIG. 3.— Incidence of damped Ly $\alpha$  systems per unit redshift  $n(z)$  as a function of redshift for the SDSS-DR1 (red points) and total samples (black points). The vertical error bars reflect  $1\sigma$  uncertainty assuming Poissonian statistics and the horizontal bars indicate the redshift interval. The dotted blue line is the fit to  $n(z)$  from Storrie-Lombardi and Wolfe (2000):  $n(z) = 0.055(1+z)^{1.11}$ .

Granted a determination of  $g(z)$ , it is trivial to calculate the number density of DLA systems per unit redshift  $n(z) \equiv N_{\text{DLA}}(z)/g(z)$ . Integrating  $n(z)$  over several redshift bins, we derive the results presented in Figure 4.1 for the SDSS-DR1 sample (red) and the combined surveys (black). Overplotted on the figure is the power-law fit to  $n(z)$  from Storrie-Lombardi and Wolfe (2000):  $n(z) = 0.055(1+z)^{1.11}$ . The SDSS-DR1 sample is in good agreement with previous analysis; this bolsters the assertion that our analysis has  $> 95\%$  completeness. The combined data sample has uncertainties in  $n(z)$  of 10 – 15% for  $\Delta z = 0.5$  intervals. With future SDSS data releases, we will measure  $n(z)$  in  $\Delta z = 0.25$  intervals to better than 5% uncertainty. This measurement provides an important constraint on the HI cross-section of high redshift galaxies (e.g. Nagamine, Springel, & Hernquist 2004a) and thereby models of galaxy formation with CDM cosmology (e.g. Kauffmann 1996; Ma et al. 1997). Table 3 lists the  $n(z)$  values for the total sample for the redshift bins shown in Figure 4.1.

##### 4.2. $\Omega_g$

We now turn our attention to the cosmological baryonic mass density in neutral gas  $\Omega_g$  as determined by DLA surveys. As first described by Wolfe (1986), one can calculate  $\Omega_g$  for a given redshift interval by summing the  $N(\text{HI})$  values of all DLA systems within that interval and comparing against the total cosmological distance  $\Delta X$  surveyed

$$\Omega_g = \frac{\mu m_H H_0}{c \rho_c} \frac{\Sigma N(\text{HI})}{\Delta X} , \quad (1)$$

where  $\mu$  is the mean molecular mass of the gas (taken to be 1/3),  $H_0$  is Hubble's constant, and  $\rho_c$  is the critical mass

TABLE 2  
SDSS DLA SAMPLE

Name	$r'$	$z_{em}$	$z_{abs}$	$\log N(\text{HI})$	Comment
J003501.88–091817	19.10	2.420	2.338	$20.55^{+0.15}_{-0.15}$	continuum
J012230.62+133437	19.32	3.010	2.349	$20.30^{+0.15}_{-0.15}$	
J012747.80+140543	18.73	2.490	2.442	$20.30^{+0.15}_{-0.15}$	continuum, blending
J013901.40–082443	18.68	3.020	2.677	$20.70^{+0.15}_{-0.15}$	
J021129.16+124110	18.87	2.950	2.595	$20.60^{+0.15}_{-0.15}$	
J022554.85+005451	18.97	2.970	2.714	$21.00^{+0.15}_{-0.15}$	blending
J023408.97–075107	18.97	2.540	2.319	$20.95^{+0.15}_{-0.15}$	
J025512.29–071107	19.43	2.820	2.612	$20.45^{+0.15}_{-0.20}$	
J025518.58+004847	19.27	3.990	3.254	$20.65^{+0.15}_{-0.15}$	continuum, blending
			3.915	$21.40^{+0.15}_{-0.15}$	continuum, blending
J033854.77–000520	18.78	3.050	2.229	$20.90^{+0.15}_{-0.15}$	continuum, blending, poor SNR
J074500.47+341731	19.25	3.710	2.995	$20.45^{+0.15}_{-0.15}$	
			3.228	$21.10^{+0.15}_{-0.15}$	
J075545.61+405643	19.23	2.350	2.301	$20.35^{+0.20}_{-0.15}$	blending
J080137.68+472528	19.42	3.280	3.223	$20.70^{+0.15}_{-0.15}$	continuum, blending
J081435.18+502946	18.34	3.880	3.708	$21.35^{+0.15}_{-0.15}$	
J081618.99+482328	19.17	3.570	2.701	$20.40^{+0.20}_{-0.15}$	continuum
			3.436	$20.80^{+0.15}_{-0.15}$	continuum
J082535.19+512706	18.36	3.510	3.318	$20.85^{+0.15}_{-0.15}$	
J082612.54+451355	19.23	3.820	3.460	$21.35^{+0.15}_{-0.15}$	blending, poor SNR
J084039.27+525504	19.34	3.090	2.862	$20.30^{+0.15}_{-0.15}$	continuum
J084407.29+515311	19.44	3.210	2.775	$21.45^{+0.15}_{-0.15}$	continuum
J090301.24+535315	18.56	2.440	2.291	$21.40^{+0.15}_{-0.15}$	
J091223.02+562128	19.09	3.000	2.889	$20.55^{+0.15}_{-0.15}$	continuum
J091955.42+551205	19.02	2.510	2.387	$20.45^{+0.15}_{-0.15}$	continuum
J092014.47+022803	19.21	2.940	2.351	$20.70^{+0.15}_{-0.15}$	continuum
J093657.14+581118	19.03	2.540	2.275	$20.35^{+0.15}_{-0.15}$	blending
J094008.44+023209	19.41	3.220	2.565	$20.70^{+0.15}_{-0.15}$	
J094759.41+632803	19.17	2.620	2.496	$20.65^{+0.15}_{-0.15}$	
J100428.43+001825	18.50	3.050	2.540	$21.00^{+0.15}_{-0.15}$	
			2.685	$21.35^{+0.15}_{-0.15}$	
J104252.32+011736	18.69	2.440	2.267	$20.75^{+0.15}_{-0.15}$	continuum, poor SNR
J104543.55+654321	19.10	2.970	2.458	$20.85^{+0.15}_{-0.15}$	continuum
J110749.14–011230	19.22	3.400	2.940	$20.80^{+0.15}_{-0.15}$	blending
J113441.22+671751	18.59	2.960	2.815	$20.40^{+0.15}_{-0.15}$	blending
J114220.26–001216	18.91	2.490	2.258	$20.35^{+0.15}_{-0.15}$	

Table 2 – cont

Name	$r'$	$z_{em}$	$z_{abs}$	$\log N(\text{HI})$	Comment
J120144.36+011611	17.53	3.230	2.684	$21.00^{+0.15}_{-0.15}$	
J120847.64+004321	19.19	2.720	2.608	$20.45^{+0.15}_{-0.15}$	
J121238.41+675920	18.68	2.570	2.221	$20.40^{+0.15}_{-0.15}$	
			2.264	$20.35^{+0.20}_{-0.20}$	
J122848.21–010414	18.23	2.660	2.263	$20.40^{+0.15}_{-0.15}$	
J122924.11–020914	19.27	3.620	2.701	$20.65^{+0.15}_{-0.15}$	
J123131.88–015350	19.30	3.900	3.670	$20.30^{+0.15}_{-0.15}$	
J125131.73+661627	19.34	3.020	2.777	$20.45^{+0.15}_{-0.15}$	
J125659.79–033813	19.08	2.970	2.434	$20.50^{+0.15}_{-0.15}$	
J125759.22–011130	18.87	4.110	4.022	$20.35^{+0.15}_{-0.15}$	
J130643.07–013552	18.82	2.940	2.773	$20.60^{+0.15}_{-0.15}$	
J133000.94+651948	18.89	3.270	2.951	$20.80^{+0.15}_{-0.15}$	blending, poor SNR
J134811.22+641348	19.12	3.840	3.555	$21.50^{+0.15}_{-0.15}$	
J135440.16+015827	19.07	3.290	2.562	$20.80^{+0.15}_{-0.15}$	
J135828.74+005811	19.40	3.910	3.020	$20.30^{+0.15}_{-0.15}$	blending
J140200.88+011751	18.81	2.950	2.431	$20.30^{+0.15}_{-0.15}$	
J140248.07+014634	18.84	4.160	3.277	$20.95^{+0.15}_{-0.15}$	
J140501.12+041535	19.31	3.220	2.708	$20.90^{+0.15}_{-0.15}$	poor SNR
J144752.47+582420	18.37	2.980	2.818	$20.65^{+0.15}_{-0.15}$	blending
J145243.61+015430	18.87	3.910	3.253	$21.45^{+0.15}_{-0.15}$	
J145329.53+002357	18.58	2.540	2.444	$20.40^{+0.15}_{-0.15}$	
J150345.94+043421	19.49	3.060	2.618	$20.40^{+0.20}_{-0.15}$	blending
J150611.23+001823	18.89	2.830	2.207	$20.30^{+0.15}_{-0.15}$	continuum
J163912.86+440813	19.22	3.770	3.642	$20.50^{+0.15}_{-0.15}$	
J164022.78+411548	19.41	3.080	2.697	$20.55^{+0.15}_{-0.15}$	
			3.017	$20.65^{+0.15}_{-0.15}$	
J165855.20+375853	19.13	3.640	3.348	$20.95^{+0.15}_{-0.15}$	continuum
J171227.74+575506	17.46	3.010	2.253	$20.60^{+0.15}_{-0.15}$	blending
J203642.29–055300	18.80	2.580	2.280	$21.20^{+0.15}_{-0.15}$	continuum, blending
J205922.42–052842	19.01	2.540	2.210	$20.90^{+0.15}_{-0.15}$	continuum, blending, poor SNR
J210025.03–064146	18.12	3.140	3.092	$21.05^{+0.15}_{-0.15}$	blending
J215117.00–070753	19.26	2.520	2.327	$20.45^{+0.15}_{-0.15}$	continuum
J230623.69–004611	19.23	3.580	3.119	$20.65^{+0.15}_{-0.15}$	continuum
J235057.87–005209	18.79	3.020	2.426	$20.55^{+0.15}_{-0.15}$	continuum, blending
			2.615	$21.20^{+0.15}_{-0.15}$	continuum, blending

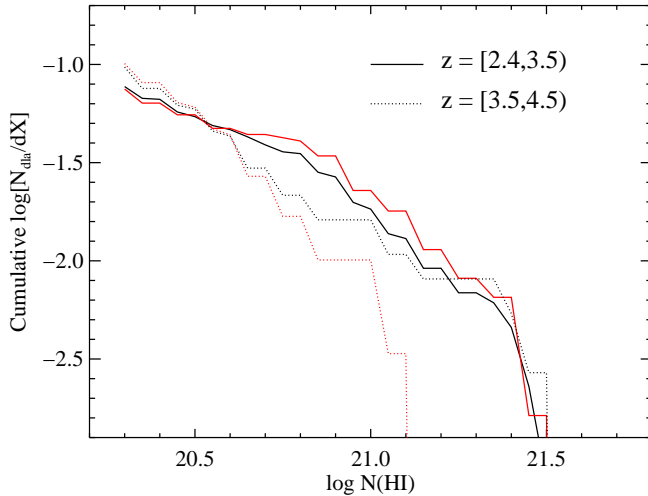


FIG. 4.— Cumulative logarithmic incidence of DLA systems per unit absorption distance interval  $dX$  as a function of  $\log N(\text{HI})$ . The red curves correspond to the DLA compilation of PMSI03 and the black curves refer to the combined sample. Note that the high redshift results have changed significantly by including the SDSS-DR1 sample.

density. We have calculated  $\Delta X$  and  $\Omega_g$  for the SDSS-DR1 sample and the PMSI03 compilation for a  $\Omega_m = 0.3$ ,  $\Omega_\Lambda = 0.7$ ,  $H_0 = 70 \text{ km s}^{-1}\text{Mpc}^{-1}$  cosmology consistent with the current ‘concordance’ cosmology (e.g. Spergel et al. 2003).

Implicit to Equation 1 is the presumption that the DLA systems dominate  $\Omega_g$  at all redshift. A principal result of PMSI03 was that at  $z > 3.5$  there are fewer DLA systems with  $N(\text{HI}) > 10^{21} \text{ cm}^{-2}$  and, therefore, that absorption systems with  $N(\text{HI}) \lesssim 10^{20} \text{ cm}^{-2}$  (the so-called sub-DLA) could contribute 50% of  $\Omega_g$ . This point is partially described by Figure 4.1 which presents the cumulative cosmological number density of DLA systems as a function of HI column density. The red curves correspond to the compilation analyzed by PMSI03; as emphasized by these authors there is a significant drop in the fraction of DLA systems with large  $N(\text{HI})$  at  $z > 3.5$  in their compilation. The authors then argued that the sub-DLA make an important contribution to  $\Omega_g$  at high redshift. The black lines in Figure 4.1 correspond to the combined sample. There is only a modest difference between the PMSI03 and combined samples for the  $z = [2.4, 3.5]$  interval, but at  $z > 3.5$  (dotted lines) the SDSS-DR1 results have greatly changed the picture<sup>2</sup>. Although the SDSS-DR1 systems contribute only 8 new DLA systems at  $z > 3.5$ , half of these have  $N(\text{HI}) > 10^{21} \text{ cm}^{-2}$ . The resulting cumulative number density at  $z > 3.5$  is now in rough agreement with the lower redshift interval. In short, *there is no longer compelling evidence that Lyman limit systems with  $N(\text{HI}) < 2 \times 10^{20} \text{ cm}^{-2}$  contribute significantly to  $\Omega_g$  at any redshift.*

Restricting our analysis of  $\Omega_g$  to the DLA systems, we

<sup>2</sup>We also note that more accurate  $N(\text{HI})$  measurements from Prochaska et al. (2003a) indicate that PMSI03 systematically underestimated several DLA systems with large  $N(\text{HI})$  value. These new results are not included in Figure 4.1, but are included in the results presented below.

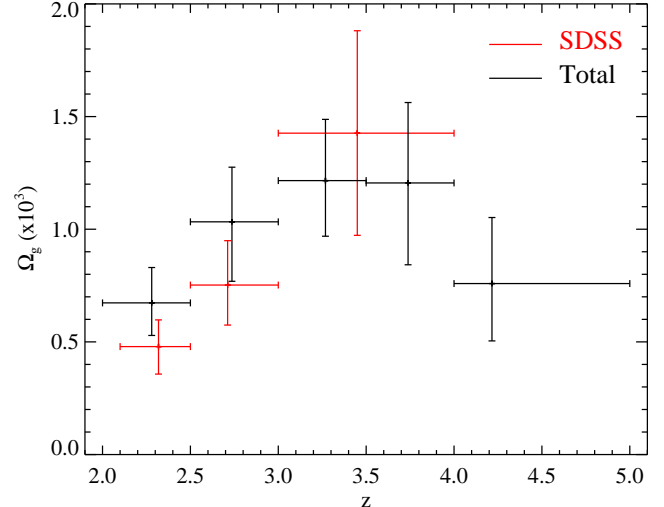


FIG. 5.— Cosmological baryonic mass density in neutral gas  $\Omega_g$  as derived from the damped Ly $\alpha$  systems for the SDSS-DR1 sample (red points) and the combined sample (black points). The  $1\sigma$  vertical error bars were derived from a modified bootstrap analysis described in the text. Contrary to previous studies,  $\Omega_g$  is rising or unchanged to  $z = 4$  and there is only a statistically insignificant decline at  $z > 4$ .

derive  $\Omega_g$  for the SDSS-DR1 sample and the combined datasets (Figure 5, Table 3). The points plotted in Figure 5 are centered at the  $N(\text{HI})$ -weighted redshift in each interval and the horizontal errors correspond to the redshift bins analyzed. It is difficult to estimate the error in  $\Omega_g$  because the uncertainty is dominated by sample size, especially the column density frequency distribution  $f(N)$  at  $N(\text{HI}) > 10^{21} \text{ cm}^{-2}$ . In the current analysis, we estimate  $1\sigma$  uncertainties through a modified bootstrap error analysis. Specifically, we examine the distribution of  $\Omega_g$  values for 1000 trials where we randomly select  $m \pm p$  DLA systems for each redshift interval containing  $m$  DLA systems and where  $p$  is a normally distributed random integer with standard deviation  $\sqrt{m}$ . The bootstrap technique provides a meaningful assessment of the uncertainty related to sample size provided the observed dataset samples a significant fraction of the intrinsic distribution. At present, we are not confident that this is the case at any redshift interval, but particularly at  $z > 3$ . The results for the  $z > 4$  redshift interval are an extreme example of this concern. The addition of one or two new DLA with  $N(\text{HI}) > 10^{21} \text{ cm}^{-2}$  would significantly increase  $\Omega_g$  and its  $1\sigma$  uncertainty. Therefore, we caution the reader that the  $1\sigma$  errors reported in Table 3 likely underestimate the true uncertainty.

Contrary to previous works, the SDSS-DR1 sample shows no evidence for a decline in  $\Omega_g$  at high redshift; the results are even suggestive of an increasing baryonic mass density at  $z > 3$ . We caution, however, that the uncertainties are large. Combining the SDSS-DR1 sample with the previous studies<sup>3</sup>, we reach a similar conclusion except at  $z > 4$  where the current results indicate a drop in  $\Omega_g$ . As noted above, the results in the highest redshift interval are very

<sup>3</sup>We have updated the measurements presented in PMSI03 to match the ones presented in Prochaska et al. (2003b).

uncertain owing to small sample size. At present, we consider it an open question as to whether  $\Omega_g$  declines at high redshift. In fact, it remains a real possibility that  $\Omega_g$  will continue to increase to  $z = 5$ .

One means of assessing the robustness of the  $\Omega_g$  values to sample size is to examine the cumulative total  $N(\text{HI})$  in the various redshift intervals. This quantity is presented in Figure 6 as a function of  $N(\text{HI})$  for the combined DLA sample. On the positive side, the total  $N(\text{HI})$  for the  $z < 4$  samples all approach  $10^{22.5} \text{ cm}^{-2}$  which is  $\approx 10 \times$  larger than the highest  $N(\text{HI})$  values observed to date. Therefore, the results in these intervals are reasonably robust to the inclusion of an ‘outlier’ with  $N(\text{HI}) \approx 10^{22} \text{ cm}^{-2}$ . On the other hand, the curves in Figure 6 demonstrate that DLA systems with  $N(\text{HI}) > 10^{21} \text{ cm}^{-2}$  do contribute  $\approx 50\%$  of the total  $N(\text{HI})$  in each interval. This point stresses the sensitivity of  $\Omega_g$  to sample size; there are relatively few DLA systems with  $N(\text{HI}) > 10^{21} \text{ cm}^{-2}$  in each interval. Until one has identified  $> 25$  DLA systems with  $N(\text{HI}) > 10^{21} \text{ cm}^{-2}$  in each interval, we fear the  $\Omega_g$  values will be subject to sample size.

## 5. SUMMARY AND CONCLUDING REMARKS

In this paper, we have introduced an automated approach for identifying DLA systems in the SDSS quasar database. We have applied our method to the Data Release 1 quasar sample and have identified a statistical sample of 71 DLA systems including  $> 50$  previously unpublished cases. Remarkably, the SDSS Data Release 1 exceeds the statistical significance of the previous two decades of DLA research at  $z \approx 2.5$ . More importantly, this sample was drawn from a well defined, homogeneous dataset of quasar spectroscopy. We present measurements of the number per unit redshift  $n(z)$  of the DLA population and the contribution of these systems to the cosmological baryonic mass density in neutral gas  $\Omega_g$ . Although the SDSS-DR1 sample does not offer a definitive assessment of either of these quantities, future SDSS data releases will provide a major advancement over all previous work.

Our measurements of  $n(z)$  are consistent with previous results suggesting a high completeness level for our DLA survey of the SDSS-DR1. Contrary to these studies, however, we find  $\Omega_g$  increases with redshift to at least  $z = 3$

TABLE 3  
RESULTS

Sample	$z$	$N$	$n(z)$	$\Delta X^a$	$\Omega_g(10^{-3})$
SDSS					
	2.1–2.5	26	$0.211 \pm 0.037$	505.0	$0.47^{+0.12}_{-0.12}$
	2.5–3.0	26	$0.254 \pm 0.046$	420.9	$0.76^{+0.20}_{-0.18}$
	3.0–4.1	19	$0.296 \pm 0.065$	266.3	$1.43^{+0.44}_{-0.45}$
Total					
	2.0–2.5	52	$0.189 \pm 0.026$	880.8	$0.67^{+0.16}_{-0.14}$
	2.5–3.0	44	$0.215 \pm 0.032$	704.5	$1.03^{+0.24}_{-0.26}$
	3.0–3.5	31	$0.271 \pm 0.049$	421.8	$1.22^{+0.27}_{-0.25}$
	3.5–4.0	25	$0.366 \pm 0.073$	268.0	$1.21^{+0.36}_{-0.36}$
	4.0–5.0	11	$0.401 \pm 0.121$	113.5	$0.76^{+0.29}_{-0.26}$

<sup>a</sup> Assumes a  $\Omega_m = 0.3, \Omega_\Lambda = 0.7, H_0 = 70 \text{ km s}^{-1} \text{ Mpc}^{-1}$  cosmology.

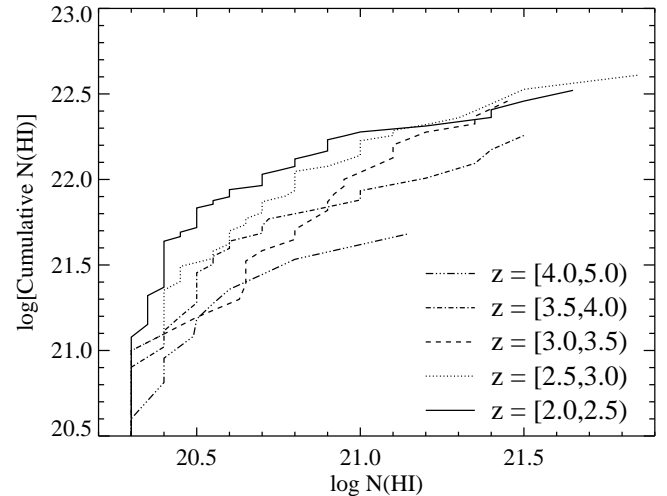


FIG. 6.— Cumulative total  $N(\text{HI})$  as a function of  $\log N(\text{HI})$  for the redshift intervals displayed in Figure 5. These curves provide a qualitative assessment of the robustness of the  $\Omega_g$  values to the addition of new DLA systems, especially ‘outliers’ with large  $N(\text{HI})$ .

and is consistent with increasing to  $z = 4$  and beyond. This latter claim, however, is subject to significant uncertainty relating to sample size. Perhaps the most important result of our analysis is that the full DLA sample no longer shows significantly fewer DLA systems with large  $N(\text{HI})$  at  $z > 3.5$ . This contradicts the principal result of PMSI03 from their analysis of the pre-SDSS DLA compilation. Apparently, their maximum likelihood approach failed to adequately assess uncertainty related to sample size. With the inclusion of only 8 new DLA, we no longer find evidence that Lyman limit systems with  $N(\text{HI}) < 2 \times 10^{20} \text{ cm}^{-2}$  are required in an analysis of  $\Omega_g$ .

Before concluding, we offer several additional criticisms of the PMSI03 analysis and the role of sub-DLA systems. First, these authors assumed a three parameter  $\Gamma$ -function for the column density frequency distribution of absorption systems with  $N(\text{HI}) > 10^{17} \text{ cm}^{-2}$ ,  $f(N) = (f_*/N_*)(N/N_*)^{-\beta} e^{-N/N_*}$ . Although this function gives a reasonable fit to the column density frequency distribution of the DLA systems, it is not physically motivated<sup>4</sup> and (more importantly) places much greater emphasis on sub-DLA than other functions (e.g. a broken power-law). Future assessments must include other functional forms to examine this systematic uncertainty. Second, the authors did not fit for the normalization of the distribution function  $f_*$ . The uncertainty in this parameter could easily contribute an additional  $> 50\%$  to the error budget. Third, their treatment did not account for sample variance; the uncertainties these authors reported were severe underestimates. Finally (and perhaps most importantly), a recent analysis of a sub-DLA sample by Dessauges-Zavadsky et al. (2003) has shown that these absorption systems have very high ionization fraction. Although these absorption systems may ultimately make an important contribution to the total HI mass density of

<sup>4</sup>In fact this curve does not smoothly connect to the power-law derived for quasar absorption lines with  $N(\text{HI}) < 10^{17} \text{ cm}^{-2}$ .

the universe, they are intrinsically different from the DLA systems. Indeed, a more appropriate title for this sub-set of Lyman limit systems is the ‘super-LLS’. This gas – in its present form – cannot contribute to star formation and is unlikely to be directly associated with galactic disks or the inner regions of protogalactic ‘clumps’. Any interpretation of results related to the super-LLS must carefully consider these points.

We acknowledge the tremendous effort put forth by the SDSS team to produce and release the SDSS survey. We thank Art Wolfe, Gabe Prochter, and Ben Weiner for helpful comments and suggestions. JXP and SHF are partially supported by NSF grant AST-0307408 and its REU subcontract.

#### REFERENCES

Abazajian, K. et al. 2003, AJ, 126, 2081  
 Burles, S.M., & Schlegel, D. 2004, in preparation  
 Dessauges-Zavadsky, M., Péroux, C., Kim, T.-S., D’Odorico, S., McMahon, R.G. 2003, MNRAS, 345, 447  
 Ellison, S.L., Yan, L., Hook, I.M., Pettini, M., Wall, J.V., & Shaver, P. 2001, A&A, 379, 393  
 Fall, S.M. & Pei, Y.C. 1993, ApJ, 402, 479  
 Kauffmann, G. 1996, MNRAS, 281, 475  
 Lanzetta, K. M., Wolfe, A. M., Turnshek, D. A., Lu, L., McMahon, R. G., & Hazard, C. 1991, ApJS, 77, 1  
 Ledoux, C., Petitjean, P., & Srianand, R. 2003, MNRAS, 396, 429  
 Lu, L., Sargent, W.L.W., Barlow, T.A., Churchill, C.W., & Vogt, S. 1996, ApJS, 107, 475  
 Ma, C.-P., Bertschinger, E., Hernquist, L., Weinberg, D.H., & Katz, N. 1997, 484, 1L  
 Mathlin, G.P., Baker, A.C., Churches, D.K., & Edmunds, M.G. 2001, MNRAS, 321, 743  
 Nagamine, K., Springel, V., & Hernquist, L. 2004, MNRAS, 348, 421  
 Nagamine, K., Springel, V., & Hernquist, L. 2004, MNRAS, 348, 435  
 Ostriker, J.P. & Heisler, J. 1984, ApJ, 278, 1  
 Pei, Y.C. & Fall, S.M. 1995, ApJ, 454, 69  
 Péroux, C., McMahon, R., Storrie-Lombardi, L., & Irwin, M.J. 2003, MNRAS, 346, 1103 (PMSS03)  
 Pettini, M., Smith, L. J., Hunstead, R. W., and King, D. L. 1994, ApJ, 426, 79  
 Prochaska, J. X. & Wolfe, A. M. 1997, ApJ, 486, 73  
 Prochaska, J.X., Howk, J.C., & Wolfe, A.M. 2003, Nature, 423, 57  
 Prochaska, J.X., Gawiser, E., Wolfe, A.M., Cooke, J., & Gelino, D. 2003, ApJS, 147, 227  
 Prochaska, J.X., Gawiser, E., Wolfe, A.M., Castro, S., & Djorgovski, S.G. 2003, ApJ, 595, L9  
 Rao, S.M. & Turnshek, D.A. 2000, ApJS, 130, 1  
 Sheinis, A.I., Miller, J., Bigelow, B., Bolte, M., Epps, H., Kibrick, R., Radovan, M., & Sutin, B. 2002, PASP, 114, 851  
 Somerville, R. S., Primack, J. R., & Faber, S.M. 2001, MNRAS, 320, 504  
 Songaila, A. & Cowie, L.L. 2002, AJ, 123, 2183  
 Storrie-Lombardi, L.J. & Wolfe, A.M. 2000, ApJ, 543, 552  
 Spergel, D. et al. 2003, ApJS, 148, 175  
 Vladilo, G. 1998, ApJ, 493, 583  
 Webb, J.K., Murphy, M.T., Flambaum, V.V., Dzuba, V.A., Barrow, J.D., Churchill, C.W., Prochaska, J.X., & Wolfe, A.M. 2001 Phys. Rev. Lett. 87, 1301  
 Wolfe, A.M. 1985, Phil. Trans. Roy. Soc. Lon., 321, 503  
 Wolfe, A.M., Turnshek, D.A., Smith, H.E., & Cohen, R.D. 1986, ApJS, 61, 249  
 Wolfe, A. M., Prochaska, J.X., & Gawiser, E. 2003, ApJ, 593, 215